

Kernel Self-Attention in Deep Multiple Instance Learning

Dawid Rymarczyk^{1,2} Jacek Tabor¹ Bartosz Zieliński^{1,2}

¹ Faculty of Mathematics and Computer Science, Jagiellonian University,
6 Łojasiewicza Street, 30-348 Kraków, Poland

² Ardigen, 76 Podole Street, 30-394 Kraków, Poland

Abstract. Multiple Instance Learning (MIL) is weakly supervised learning, which assumes that there is only one label provided for the entire bag of instances. As such, it appears in many problems of medical image analysis, like the whole-slide images classification of biopsy. Most recently, MIL was also applied to deep architectures by introducing the aggregation operator, which focuses on crucial instances of a bag. In this paper, we enrich this idea with the self-attention mechanism to take into account dependencies across the instances. We conduct several experiments and show that our method with various types of kernels increases the accuracy, especially in the case of non-standard MIL assumptions. This is of importance for real-word medical problems, which usually satisfy presence-based or threshold-based assumptions.

Keywords: Multiple Instance Learning · Deep Learning · Cancer Classification

1 Introduction

Classification methods typically assume that there exists a separate label for each example from a dataset. However, in many real-life applications, there exists only one label for a bag of instances because it is too laborious to label all of them separately. This type of problem, called Multiple Instance Learning (MIL) [5], assumes that there is only one label provided for the entire bag and that some of the instances associate to this label [6].

MIL problems are common in medical image analysis due to the vast resolution of images or the weakly labeled datasets. Among others, they appear in the whole slide-images classification of biopsies [2, 3, 24], classification of dementia in brain MRI [20], or the diabetic retinopathy screening [16].

Recently, Ilse et al. [9] introduced the Attention-based MIL Pooling (Ab-MILP), a trainable operator that aggregates information from multiple instances of a bag. It bases on a two-layered neural network with the attention weights, which allow finding the essential instances. Since the publication, this mechanism was widely adopted in the medical image analysis [13, 15, 23], especially for the assessment of whole-slide images. However, the Attention-based MIL Pooling is significantly different from the Self-Attention (SA) mechanism [25]. It perfectly

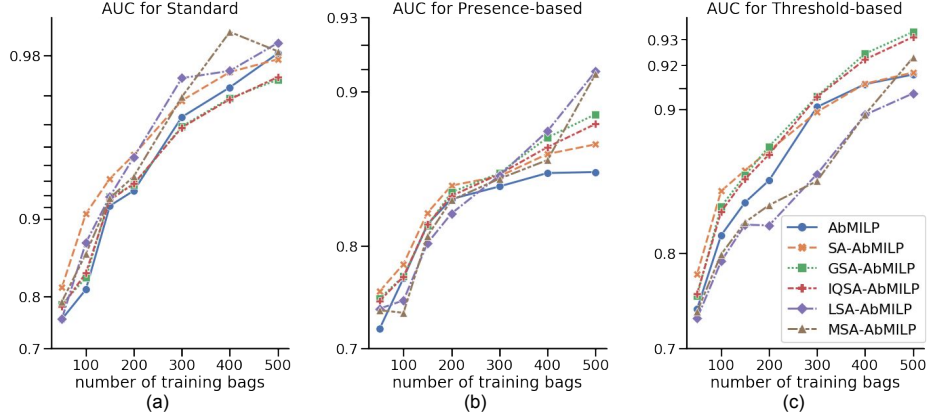


Fig. 1: Results for MNIST dataset with bags generated using standard (a), presence-based (b), and threshold-based (c) assumption. In all cases, our approach, either with dot product (SA-AbMILP) or the other kernels (GSA-AbMILP, IQSA-AbMILP, LSA-AbMILP, and MSA-AbMILP) obtains statistically better results than the baseline method (AbMILP). See Section 3 for description of the shortcuts.

aggregates information from a varying number of instances. However, it does not model dependencies between them.

In this work, we introduce a method that combines Self-Attention with Attention-based MIL Pooling. It simultaneously catches the global dependencies between the instances in the bag and aggregates them into a fixed-sized vector required for the successive layers of the network. Moreover, we investigate a broad spectrum of kernels replacing dot product. According to the results of the experiments, using our method with various kernels is beneficial compared to the AbMILP approach, especially in the case of more challenging MIL assumptions. Our code is publicly available at ***.

2 Multiple Instance Learning

Multiple Instance Learning (MIL) is a variant of inductive machine learning belonging to the supervised learning paradigm [6]. In a typical supervised problem, a separate feature vector exists for each sample: $\mathbf{x} = \mathbf{h}, \mathbf{h} \in \mathbb{R}^{L \times 1}$. In MIL, each example is represented by a bag of feature vectors called instances: $\mathbf{x} = \{\mathbf{h}_i\}_{i=1}^N, \mathbf{h}_i \in \mathbb{R}^{L \times 1}$. Moreover, in *standard MIL assumption*, bag's label $\mathbf{y} \in \{0, 1\}$, each instance h_i has a hidden binary label $y_i \in \{0, 1\}$, and the bag is positive if at least one of its instances is positive:

$$\mathbf{y} = \begin{cases} 0, & \text{iff } \sum_{i=1}^N y_i = 0, \\ 1, & \text{otherwise.} \end{cases} \quad (1)$$

The standard assumptions (considered by AbMILP) is very strict and hence does not fit to numerous real-world problems. For example, in digestive track assessment using the NHI score [14], some of the criteria rely on the simultaneous presence of two inflammatory changes (e.g. infiltration of epithelium and lamina propria with neutrophils). Such a task requires more challenging types of MIL called presence-based or threshold-based assumptions [6] (defined below), which operate on multiple assumptions (called concepts) and classes.

Let $\hat{C} \subseteq C$ be the set of required instance-level concepts, and let $p : X \times C \rightarrow K$ be the function that counts how often the concept $c \in C$ occurs in the bag $\mathbf{x} \in X$. Then, in *presence-based assumption*, the bag is positive if each concept occurs at least ones:

$$\mathbf{y} = \begin{cases} 1, & \text{iff for each } c \in \hat{C} : p(\mathbf{x}, c) \geq 1, \\ 0, & \text{otherwise.} \end{cases} \quad (2)$$

In the case of *threshold-based assumptions*, the bag is positive if concept $c_i \in C$ occurs at least $t_i \in \mathbb{N}$ times:

$$\mathbf{y} = \begin{cases} 1, & \text{iff for each } c_i \in \hat{C} : p(\mathbf{x}, c_i) \geq t_i, \\ 0, & \text{otherwise.} \end{cases} \quad (3)$$

In this paper, we introduce methods suitable not only for the standard assumption (like AbMILP) but also for presence-based and threshold-based assumptions.

3 Methods

3.1 Attention-based Multiple Instance Learning Pooling

Attention-based MIL Pooling (AbMILP) [9] is a type of weighted average pooling, where the neural network determines the weights of instances. More formally, if the bag $\mathbf{x} = \{\mathbf{h}_i\}_{i=1}^N$, $\mathbf{h}_i \in \mathbb{R}^{L \times 1}$, then the output of the operator is defined as:

$$\mathbf{z} = \sum_{i=1}^N a_i \mathbf{h}_i, \text{ where } a_i = \frac{\exp(\mathbf{w}^T \tanh(\mathbf{V} \mathbf{h}_i))}{\sum_j^N \exp(\mathbf{w}^T \tanh(\mathbf{V} \mathbf{h}_j))}, \quad (4)$$

$\mathbf{w} \in \mathbb{R}^{M \times 1}$ and $\mathbf{V} \in \mathbb{R}^{M \times L}$ are trainable layers of neural networks, and hyperbolic tangent prevents the exploding gradient. Moreover, the weights a_i sum up to 1 to wean from various sizes of the bags.

The most important limitation of AbMILP is the assumption that all instances of the bag are independent. To overcome this limitation, we extend it by introducing the *self-attention mechanism* (SA) [25], which models dependencies between instances of the bag.

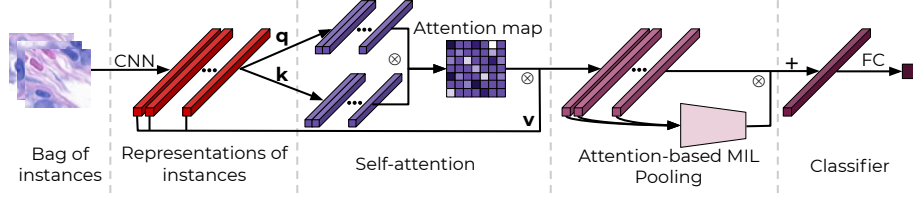


Fig. 2: The pipeline of self-attention in deep MIL starts with obtaining feature space representation for each of the instances from the bag using features block of Convolutional Neural Network (CNN). In order to model dependencies between the instances, their representations pass through the self-attention layer and then aggregate using AbMILP operator. The obtained fixed-size vector goes through the Fully Connected (FC) classification layer.

3.2 Self-Attention in Multiple Instance Learning

The pipeline of our method consists of four steps. First, the bag (e.g. fragments of the image) goes through the Convolutional Neural Network (CNN) in order to obtain representations for the instances. Those representations are used by the self-attention module (with dot product or the other kernels) to integrate dependencies of the instances into the process. Feature vectors with integrated dependencies are used as the input for the AbMILP module to obtain one fixed-sized vector for each bag. Such a vector can be passed to the successive Fully-Connected (FC) layers of the network. The whole pipeline is presented in Fig. 2. In order to make this method self-contained, below, we describe self-attention and particular kernels.

Self-Attention (SA) transforms all the instances into two feature spaces of keys $\mathbf{k}_i = \mathbf{W}_k \mathbf{h}_i$ and queries $\mathbf{q}_j = \mathbf{W}_q \mathbf{h}_j$, and calculates:

$$\beta_{j,i} = \frac{\exp(s_{ij})}{\sum_{i=1}^N \exp(s_{ij})}, \text{ where } s_{ij} = \langle \mathbf{k}(\mathbf{h}_i), \mathbf{q}(\mathbf{h}_j) \rangle, \quad (5)$$

to indicate the extent to which the model attends to the i^{th} instance when synthesizing the j^{th} one. The output of the attention layer is defined separately for each instance as:

$$\hat{\mathbf{h}}_j = \gamma \mathbf{o}_j + \mathbf{h}_j, \text{ where } \mathbf{o}_j = \sum_{i=1}^N \beta_{j,i} \mathbf{W}_v \mathbf{h}_i, \quad (6)$$

$\mathbf{W}_q, \mathbf{W}_k \in \mathbb{R}^{\bar{L} \times L}$, $\mathbf{W}_v \in \mathbb{R}^{L \times L}$ are trainable layers, $\bar{L} = L/8$, and γ is a trainable scalar initialized to 0.

Kernels in self-attention. In order to indicate to which extent one instance attends on synthesizing the other one, the self-attention mechanism typically employs a dot product (see s_{ij} in 5). However, it can be replaced by various kernels,

which is justified by the positive outcomes of such solutions observed in Support Vectors Machine (SVM) [1] or Convolutional Neural Networks (CNN) [22], especially in the case of small training sets. The Radial Basis Function (RBF) and Laplace kernels were already successfully adopted to self-attention [10, 21]. Hence, in this study, we additionally extend our approach with the following standard choice of kernels:

- Radial Basis Function (GSA-AbMILP): $k(x, y) = \exp(-\alpha\|x - y\|_2^2)$,
- Inverse quadratic (IQSA-AbMILP): $k(x, y) = \frac{1}{\alpha\|x - y\|_2^2 + 1}$,
- Laplace (LSA-AbMILP): $k(x, y) = -\|x - y\|_1$,
- Module (MSA-AbMILP): $k(x, y) = \|x - y\|^\alpha - \|x\|^\alpha - \|y\|^\alpha$.

We decided to concentrate on those kernels because they are complementary with regard to the shape of tails in their distributions. In our experiments, we treat α as a trainable parameter.

4 Experiments

We adopt three datasets to investigate the performance of our method, MNIST [12] and two medical databases of colon [18] and breast [7] cancer. For MNIST, we adapt LeNet5 [12] architecture, while for both medical datasets, SC-CNN [18] is applied. Moreover, in the case of the latter, we apply extensive data augmentation. All of the experiments are repeated 5 times using 10 fold cross-validation, including 1 validation fold and 1 test fold. We use the early stopping mechanism with 5 epochs window for MNIST and 25 epochs window for medical datasets. We use Nvidia GeForce RTX 2080 for computations.

4.1 MNIST Dataset

Experiment details. As there exists no standard benchmark for deep MIL, we first construct various types of bags based on the MNIST dataset. Each bag contains a random number of MNIST images (drawn from Gaussian distributions $\mathcal{N}(10, 2)$). We adopt three types of bag labels referring to three types of MIL assumptions:

- Standard assumptions: $\mathbf{y} = 1$ if there is at least one occurrence of “9”,
- Presence-based assumptions: $\mathbf{y} = 1$ if there is at least one occurrence of “9” and at least one occurrence of “7”,
- Threshold-based assumptions: $\mathbf{y} = 1$ if there are at least two occurrences of “9”.

We decided to use “9” and “7” because they are often confused with each other, what makes the task more challenging.

We investigated how the performance of the model depends on the number of bags used in training (we consider 50, 100, 150, 200, 300, 400, and 500 training bags). For all experiments, we use LeNet5 [12] initialized according to [8] with

the bias set to 0. We use Adam optimizer [11] with parameters $\beta_1 = 0.9$ and $\beta_2 = 0.999$, learning rate 10^{-5} , and batch size 1. And we compare the performance of our method (further called SA-AbMILP) and its kernel variations with Attention-based MIL Pooling [9].

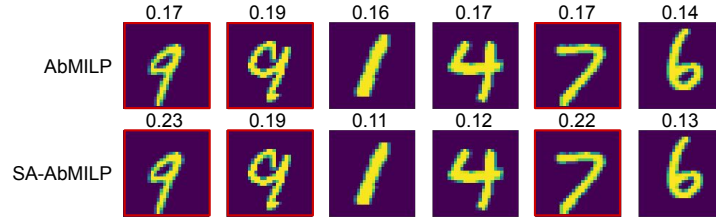


Fig. 3: Example of instances’ weights for a positive bag in a presence-based assumption (where positive is at least one occurrence of “9” and “7”) for AbMILP and our method. One can observe that in SA-AbMILP, “9”s and “7”s strengthen each other in the self-attention module, resulting in higher weights in the aggregation operator.

Results. AUC values for considered MIL assumptions are visualized in Fig. 1. One can observe that our method with a dot product (SA-AbMILP) always outperforms other methods in case of small datasets. However, when the number of training examples reaches 300, its kernel extensions work best (Laplace in presence-based and inverse quadratic in threshold-based assumption). Hence, we conclude that for small datasets, no kernel extensions should be applied, while in the case of a larger dataset, a kernel should be optimized together with the other hyperparameters. Additionally, we analyze differences between the weights of instances in AbMILP and our method. As presented in Fig. 3, our method strengthens the concepts of MIL more effectively than AbMILP, which in our opinion, is the main reason of the improved scores.

4.2 Medical Datasets

Experiment details. In the second experiment, we consider two medical datasets of *breast* and *colon* cancer (described below). For both of them, we generate instance representations using SC-CNN [18] initialized according to [8] with the bias set to 0. We use Adam [11] optimizer with parameters $\beta_1 = 0.9$ and $\beta_2 = 0.999$, learning rate 10^{-4} , and batch size 1. And we apply extensive data augmentation, including random rotations, horizontal and vertical flipping, random staining augmentation [9], staining normalization [19], and instance normalization.

Breast cancer dataset [7] contains 58 weakly labeled H&E biopsy images of resolution 896×768 . The image is labeled as malignant if it contains at least one cancer cell. Otherwise, it is labeled as benign. Each image is divided into patches of resolution 32×32 , resulting in 672 patches per image. Patches with at least 75% of the white pixels are discarded, generating 58 bags of various sizes.

Colon cancer dataset [18] contains 100 images with 22444 nuclei manually assigned to one of the following classes: epithelial, inflammatory, fibroblast, and miscellaneous. We construct bags of 27×27 patches with centers located in the nuclei's centers. The bag has a positive label if there are at least one epithelium nuclei in the bag. Tagging epithelium nuclei is essential in the case of colon cancer because the disease originates from them [17].

Table 1: Results for breast and colon cancer datasets (mean and std over 5 repetitions). See Section 3 for description of the shortcuts.

breast cancer dataset					
	accuracy	precision	recall	F-score	AUC
AbMILP	71.7 ± 2.7	77.1 ± 4.1	68.6 ± 3.9	66.5 ± 3.1	85.6 ± 2.2
SA-AbMILP	75.0 ± 2.5	77.3 ± 3.7	74.9 ± 3.7	69.8 ± 3.0	86.2 ± 2.2
GSA-AbMILP	75.8 ± 2.1	79.3 ± 3.3	74.7 ± 3.4	72.5 ± 2.5	85.9 ± 2.2
IQSA-AbMILP	76.7 ± 2.2	78.6 ± 2.3	75.1 ± 4.2	66.7 ± 4.1	85.9 ± 2.1
LSA-AbMILP	65.5 ± 2.9	62.5 ± 3.7	89.5 ± 2.6	68.5 ± 2.6	86.7 ± 2.1
MSA-AbMILP	73.8 ± 2.6	78.4 ± 3.9	73.8 ± 3.6	69.4 ± 3.4	85.8 ± 2.2
colon cancer dataset					
	accuracy	precision	recall	F-score	AUC
AbMILP	89.4 ± 1.3	95.3 ± 1.5	84.6 ± 3.0	87.2 ± 2.1	97.3 ± 0.7
SA-AbMILP	90.8 ± 1.3	93.8 ± 2.0	87.2 ± 2.4	89.0 ± 1.9	98.1 ± 0.7
GSA-AbMILP	88.4 ± 1.7	95.2 ± 1.7	83.7 ± 2.8	87.1 ± 2.2	98.5 ± 0.6
IQSA-AbMILP	89.0 ± 1.9	93.9 ± 2.1	85.5 ± 2.9	86.9 ± 2.5	96.6 ± 1.1
LSA-AbMILP	84.7 ± 1.7	92.7 ± 3.2	71.6 ± 4.7	73.4 ± 4.3	95.5 ± 1.7
MSA-AbMILP	89.6 ± 1.6	94.6 ± 1.6	85.7 ± 2.7	87.4 ± 1.8	98.4 ± 0.5

Results for medical datasets are presented in Table 1. For both of them, our method (with or without kernel extension) improves the Area Under the ROC Curve (AUC) comparing to the baseline method. Moreover, our method obtains the highest recall, which is of importance for reducing the number of false negatives. To explain why our method surpasses the AbMILP, we compare the weights of patches in the average pooling. Those patches contribute most to the final score and should be investigated by the medical doctors. One can observe in Fig. 8 that our method highlights fewer patches than AbMILP, which

simplifies their analysis. Additionally, SA dependencies obtained for the most relevant patch of our method are justified medically, as they mostly focus on nuclei located in the neighborhood of crypts (see supplementary materials for more examples). Moreover, in the case of the colon cancer dataset, we further observe the positive aspect of our method, as it strengthens epithelium nuclei and, at the same time, weakens nuclei in the lamina propria. Finally, we notice that kernels often improve overall performance without significant superiority of any of them.

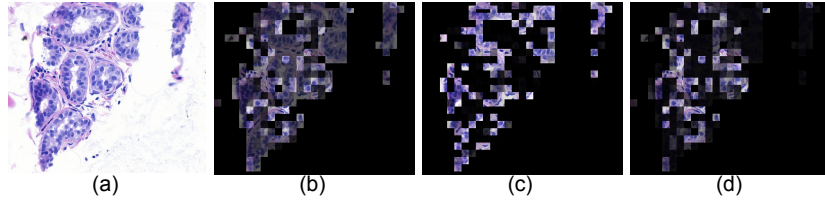


Fig. 4: An example image from the breast cancer dataset (a), weights of patches obtained by AbMILP (b) and SA-AbMILP (c), and SA dependencies obtained for the most relevant patch in SA-AbMILP (d). One can observe that SA-AbMILP highlights fewer patches than AbMILP, which simplifies their analysis. Additionally, SA dependencies are justified medically, as they mostly focus on nuclei located in the neighborhood of crypts.

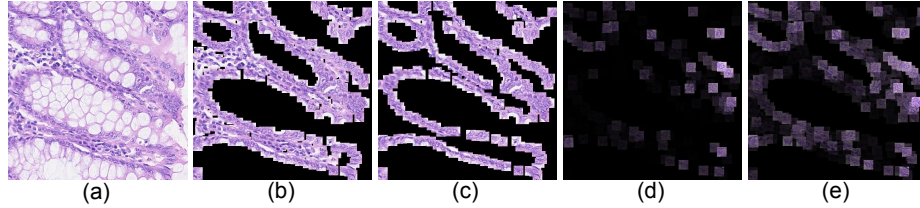


Fig. 5: An example image from the colon cancer dataset (a) with annotated nuclei (b) and epithelium nuclei (c), as well as, the weights of patches obtained by AbMILP (d) and SA-AbMILP (e). One can observe that SA-AbMILP strengthens epithelium nuclei and, at the same time, weakens nuclei in the lamina propria.

5 Conclusions and Discussion

In this paper, we propose Self-Attention for Attention-based MIL Pooling (SA-AbMILP), which combines the multi-level dependencies across image regions

with the trainable operator of weighted average pooling. In contrast to Attention-based MIL Pooling (AbMILP), it covers not only the standard but also the presence-based and threshold-based assumptions of MIL. The experiments on three datasets (MNIST and two medical datasets of breast and colon cancer) confirm that our method is on par or outperforms current state-of-the-art methodology. We demonstrate that in the case of bigger datasets, it is advisable to use various kernels of the Self-Attention instead of the commonly used dot product. We also provide qualitative results to illustrate the improvements achieved by our method.

The experiments show that methods covering a wider range of MIL assumptions fit better for real-world problems. Therefore, in future work, we plan to introduce methods for more complicated MIL assumptions [6] and apply them to more challenging tasks, like digestive track assessment using the NHI score [14]. Moreover, we plan to introduce better interpretability, using one of the most recent approaches [4].

References

1. Baudat, G., Anouar, F.: Kernel-based methods and function approximation. In: IJCNN'01. International Joint Conference on Neural Networks. Proceedings (Cat. No. 01CH37222). vol. 2, pp. 1244–1249. IEEE (2001)
2. Campanella, G., Hanna, M.G., Geneslaw, L., Mirafior, A., Silva, V.W.K., Busam, K.J., Brogi, E., Reuter, V.E., Klimstra, D.S., Fuchs, T.J.: Clinical-grade computational pathology using weakly supervised deep learning on whole slide images. *Nature medicine* **25**(8), 1301–1309 (2019)
3. Campanella, G., Silva, V.W.K., Fuchs, T.J.: Terabyte-scale deep multiple instance learning for classification and localization in pathology. *arXiv preprint arXiv:1805.06983* (2018)
4. Chen, C., Li, O., Tao, D., Barnett, A., Rudin, C., Su, J.K.: This looks like that: deep learning for interpretable image recognition. In: *Advances in Neural Information Processing Systems*. pp. 8928–8939 (2019)
5. Dietterich, T.G., Lathrop, R.H., Lozano-Pérez, T.: Solving the multiple instance problem with axis-parallel rectangles. *Artificial intelligence* **89**(1-2), 31–71 (1997)
6. Foulds, J., Frank, E.: A review of multi-instance learning assumptions. *The Knowledge Engineering Review* **25**(1), 1–25 (2010)
7. Gelasca, E.D., Byun, J., Obara, B., Manjunath, B.: Evaluation and benchmark for biological image segmentation. In: *2008 15th IEEE International Conference on Image Processing*. pp. 1816–1819. IEEE (2008)
8. Glorot, X., Bengio, Y.: Understanding the difficulty of training deep feedforward neural networks. In: *Proceedings of the thirteenth international conference on artificial intelligence and statistics*. pp. 249–256 (2010)
9. Ilse, M., Tomczak, J.M., Welling, M.: Attention-based deep multiple instance learning. *arXiv preprint arXiv:1802.04712* (2018)
10. Kim, H., Mnih, A., Schwarz, J., Garnelo, M., Eslami, A., Rosenbaum, D., Vinyals, O., Teh, Y.W.: Attentive neural processes. *arXiv preprint arXiv:1901.05761* (2019)
11. Kingma, D.P., Ba, J.: Adam: A method for stochastic optimization. *arXiv preprint arXiv:1412.6980* (2014)

12. LeCun, Y., Bottou, L., Bengio, Y., Haffner, P.: Gradient-based learning applied to document recognition. *Proceedings of the IEEE* **86**(11), 2278–2324 (1998)
13. Li, J., Li, W., Gertych, A., Knudsen, B.S., Speier, W., Arnold, C.W.: An attention-based multi-resolution model for prostate whole slide imageclassification and localization. *arXiv preprint arXiv:1905.13208* (2019)
14. Li, K., Strauss, R., Marano, C., Greenbaum, L.E., Friedman, J.R., Peyrin-Biroulet, L., Brodmerkel, C., De Hertogh, G.: A simplified definition of histologic improvement in ulcerative colitis and its association with disease outcomes up to 30 weeks from initiation of therapy: Post hoc analysis of three clinical trials. *Journal of Crohn's and Colitis* **13**(8), 1025–1035 (2019)
15. Lu, M.Y., Chen, R.J., Wang, J., Dillon, D., Mahmood, F.: Semi-supervised histology classification using deep multiple instance learning and contrastive predictive coding. *arXiv preprint arXiv:1910.10825* (2019)
16. Quéllec, G., Lamard, M., Abramoff, M.D., Decencière, E., Lay, B., Erginay, A., Cochener, B., Cazuguel, G.: A multiple-instance learning framework for diabetic retinopathy screening. *Medical image analysis* **16**(6), 1228–1240 (2012)
17. Ricci-Vitiani, L., Lombardi, D.G., Pilozzi, E., Biffoni, M., Todaro, M., Peschle, C., De Maria, R.: Identification and expansion of human colon-cancer-initiating cells. *Nature* **445**(7123), 111–115 (2007)
18. Sirinukunwattana, K., Raza, S.E.A., Tsang, Y.W., Snead, D.R., Cree, I.A., Rajpoot, N.M.: Locality sensitive deep learning for detection and classification of nuclei in routine colon cancer histology images. *IEEE transactions on medical imaging* **35**(5), 1196–1206 (2016)
19. Tomczak, J.M., Ilse, M., Welling, M., Jansen, M., Coleman, H.G., Lucas, M., de Laat, K., de Bruin, M., Marquering, H., van der Wel, M.J., et al.: Histopathological classification of precursor lesions of esophageal adenocarcinoma: A deep multiple instance learning approach (2018)
20. Tong, T., Wolz, R., Gao, Q., Guerrero, R., Hajnal, J.V., Rueckert, D., Initiative, A.D.N., et al.: Multiple instance learning for classification of dementia in brain mri. *Medical image analysis* **18**(5), 808–818 (2014)
21. Tsai, Y.H.H., Bai, S., Yamada, M., Morency, L.P., Salakhutdinov, R.: Transformer dissection: An unified understanding for transformer's attention via the lens of kernel. *arXiv preprint arXiv:1908.11775* (2019)
22. Wang, C., Yang, J., Xie, L., Yuan, J.: Kervolutional neural networks. In: *Proceedings of the IEEE Conference on Computer Vision and Pattern Recognition*. pp. 31–40 (2019)
23. Wang, S., Zhu, Y., Yu, L., Chen, H., Lin, H., Wan, X., Fan, X., Heng, P.A.: Rmdl: Recalibrated multi-instance deep learning for whole slide gastric image classification. *Medical image analysis* **58**, 101549 (2019)
24. Yoshida, H., Shimazu, T., Kiyuna, T., Marugame, A., Yamashita, Y., Cosatto, E., Taniguchi, H., Sekine, S., Ochiai, A.: Automated histological classification of whole-slide images of gastric biopsy specimens. *Gastric Cancer* **21**(2), 249–257 (2018)
25. Zhang, H., Goodfellow, I., Metaxas, D., Odena, A.: Self-attention generative adversarial networks. *arXiv preprint arXiv:1805.08318* (2018)

Supplementary Materials

Table 2: Results for MNIST datasets (mean and std over 5 repetitions). See Section 3 in the article for description of the shortcuts.

Standard MIL assumption							
Number of training bags	50	100	150	200	300	400	500
AbMILP	76.0 \pm 2.7	81.2 \pm 3.2	91.1 \pm 2.0	92.3 \pm 2.1	96.3 \pm 0.7	97.2 \pm 0.6	98.0 \pm 0.6
SA-AbMILP	81.5 \pm 2.5	90.5 \pm 2.0	93.2 \pm 1.5	94.6 \pm 1.4	96.8 \pm 0.8	97.6 \pm 0.6	97.9 \pm 0.7
GSA-AbMILP	78.7 \pm 2.5	83.0 \pm 2.5	91.9 \pm 1.8	92.8 \pm 1.7	95.9 \pm 0.8	96.9 \pm 0.8	97.4 \pm 0.9
IQSA-AbMILP	78.3 \pm 2.6	83.7 \pm 2.1	91.6 \pm 1.8	92.8 \pm 1.8	95.9 \pm 0.8	96.9 \pm 0.8	97.5 \pm 0.8
MSA-AbMILP	79.2 \pm 2.5	86.2 \pm 3.9	91.8 \pm 1.4	93.3 \pm 0.5	97.0 \pm 0.5	98.4 \pm 0.3	98.1 \pm 0.6
LSA-AbMILP	76.1 \pm 2.9	87.5 \pm 2.9	91.9 \pm 1.4	94.5 \pm 1.3	97.5 \pm 0.5	97.7 \pm 0.8	98.2 \pm 0.5
Presence-based MIL assumption							
Number of training bags	50	100	150	200	300	400	500
AbMILP	72.1 \pm 4.8	77.2 \pm 4.6	81.8 \pm 4.0	83.7 \pm 2.7	84.5 \pm 1.9	85.4 \pm 1.9	85.5 \pm 1.3
SA-AbMILP	75.9 \pm 4.0	78.4 \pm 4.5	82.6 \pm 3.8	84.6 \pm 2.2	85.2 \pm 2.1	86.6 \pm 2.8	87.2 \pm 2.9
GSA-AbMILP	75.2 \pm 4.1	77.3 \pm 4.7	81.7 \pm 3.6	84.1 \pm 2.7	85.4 \pm 2.5	87.6 \pm 2.2	88.9 \pm 1.9
IQSA-AbMILP	75.0 \pm 4.2	77.3 \pm 4.7	81.8 \pm 3.7	83.9 \pm 2.8	85.4 \pm 2.5	87.1 \pm 2.2	88.4 \pm 2.0
MSA-AbMILP	74.1 \pm 2.9	73.8 \pm 3.7	80.8 \pm 4.0	83.6 \pm 2.4	85.1 \pm 2.2	86.3 \pm 2.5	90.8 \pm 2.9
LSA-AbMILP	74.2 \pm 2.7	75.0 \pm 3.5	80.2 \pm 3.1	82.6 \pm 2.0	85.3 \pm 3.0	88.0 \pm 3.0	90.9 \pm 2.8
Threshold-based MIL assumption							
Number of training bags	50	100	150	200	300	400	500
AbMILP	74.5 \pm 5.8	81.5 \pm 4.3	84.2 \pm 3.1	85.8 \pm 2.7	90.1 \pm 1.7	91.2 \pm 2.2	91.6 \pm 2.1
SA-AbMILP	78.0 \pm 5.4	85.0 \pm 4.3	86.4 \pm 2.9	87.7 \pm 2.8	89.9 \pm 2.4	91.2 \pm 2.4	91.7 \pm 2.3
GSA-AbMILP	75.9 \pm 6.2	83.9 \pm 3.5	86.1 \pm 3.1	87.9 \pm 2.6	90.6 \pm 2.2	92.5 \pm 2.6	93.3 \pm 2.4
IQSA-AbMILP	76.1 \pm 6.2	83.5 \pm 3.5	85.9 \pm 3.1	87.5 \pm 2.5	90.6 \pm 2.2	92.3 \pm 2.6	93.1 \pm 2.4
MSA-AbMILP	74.2 \pm 5.7	79.9 \pm 4.9	82.6 \pm 4.0	84.0 \pm 3.6	85.7 \pm 4.0	89.7 \pm 3.5	92.3 \pm 2.6
LSA-AbMILP	73.5 \pm 5.6	79.2 \pm 3.8	82.4 \pm 4.1	82.4 \pm 3.5	86.2 \pm 3.0	89.7 \pm 3.1	90.8 \pm 3.0

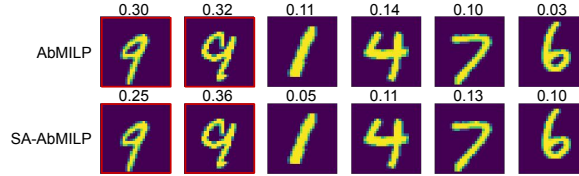


Fig. 6: Bag of instances' weights for a positive bag in a standard-based assumption (where positive is at least one occurrence of "9") for AbMILP and our method.

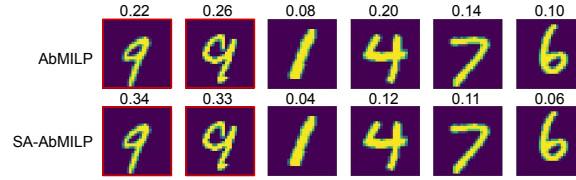


Fig. 7: Bag of instances' weights for a positive bag in a threshold-based assumption (where positive is at least two occurrences of "9") for AbMILP and our method.

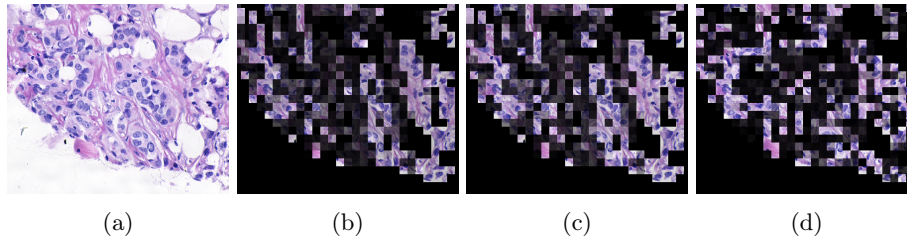


Fig. 8: An image from the breast cancer dataset (a), patches weights obtained by AbMILP (b) and SA-AbMILP (c), and SA map for the most relevant patch in SA-AbMILP (d). One can observe that SA-AbMILP covers larger area than AbMILP. Additionally, SA map mostly focus on nuclei like neutrophils and monocytes.

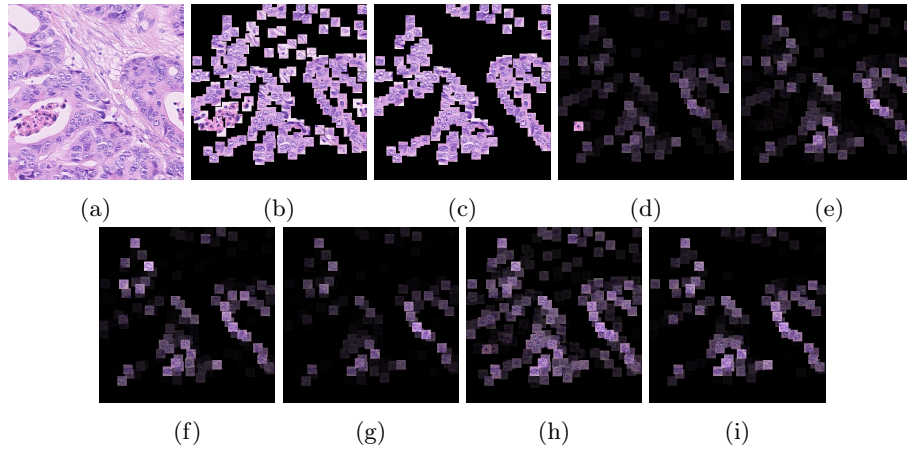


Fig. 9: An image from the colon cancer dataset (a) with nuclei (b), epithelium nuclei (c), the patches weights obtained by AbMILP (d) and SA-AbMILP (e). Additionally, we present weights for RBF (f), inverse quadratic (g), Laplace (h), and module (i) kernels. One can observe that the Laplace kernel distributes uniformly, while the inverse quadratic limits to the smallest number of the nuclei.